

---

Oral presentation | Turbulence simulation (DNS,LES,RANS)

## Turbulence simulation(DNS,LES,RANS)-V

Fri. Jul 19, 2024 10:45 AM - 12:45 PM Room B

---

### [13-B-01] Computational Modelling of Heat Convection using Liquid Metals

\*Ningshu Li<sup>1,2,3,4</sup>, Haotian He<sup>1,2,3,4</sup>, Hector Iacovides<sup>1,2,3,4</sup>, Timothy Craft<sup>1,2,3,4</sup> (1. Thermo-Fluids Group, 2. Faculty of Science and Engineering, 3. Department of Mechanical, Aerospace and Civil Engineering, 4. The University of Manchester)

Keywords: Low Prandtl number, Reynolds Averaged Navier-Stokes (RANS), Turbulent heat transfer, Forced convection

# Computational Modelling of Heat Convection using Liquid Metals

Ningshu Li\*, Haotian He\*, Hector Iacovides\* and Timothy Craft\*

Corresponding author: ningshu.li@student.manchester.ac.uk

\* Thermo-Fluids Group, The University of Manchester, Manchester M13 9PL, UK.

**Abstract:** Liquid metals are commonly used as nuclear reactor coolants to maintain the core temperature within a safe range. Their low Prandtl numbers indicate high molecular thermal conductivity, which enhances heat transfer capabilities. However, most turbulent heat flux models, based on eddy-diffusivity approaches with the constant turbulent Prandtl number, have been developed for fluids with  $Pr \sim 1$  and may not perform well for simulating liquid metals. The present paper addresses the issue by thoroughly assessing a proposed  $Pr_t$  model through computations of forced convection flows in three different geometries with various low Prandtl number fluids.

Low- $Re$  turbulence models were tested in all cases. The proposed  $Pr_t$  model was derived from a DNS database of thermal channel flow at moderate and low molecular Prandtl numbers [1]. Initially, a study was conducted on flow and heat transfer in a 2-D fully developed turbulent straight channel. Reynolds numbers of  $Re = 2846, 10200, 23000,$  and  $48500$ , along with Prandtl numbers ranging from  $Pr = 0.007$  to  $0.71$ , were simulated. The constant turbulent Prandtl number and Kays correlation [2] were compared with the proposed  $Pr_t$  model. Results from dynamic and thermal fields indicated good agreement with DNS data, particularly at higher Reynolds numbers. Testing was also conducted on a backward-facing step flow in a turbulent forced convection regime at  $Re = 4805$ , with a range of low Prandtl numbers. The proposed  $Pr_t$  model, which includes a modified Yap term weakening the effect of the standard Yap term, presented improved prediction accuracy compared to DNS results [3]. Lastly, for an impinging jet at  $Re = 5700$ , the modified Yap term and proposed  $Pr_t$  model demonstrated superior thermal performance to other models tested at  $Pr = 0.01$  and  $0.1$  compared to DNS results [4].

Based on the findings from simulations across various geometries and flow conditions, the proposed  $Pr_t$  model with the L-S  $k - \varepsilon$  turbulence model, validated against DNS data, demonstrates robust performance in predicting thermal characteristics in turbulent flows with low Prandtl numbers.

*Keywords:* Turbulent Heat Transfer, Computational Fluid Dynamics, RANS Modeling, Low Prandtl fluids.

## 1 Introduction

Liquid metals are being considered coolants for the Generation IV nuclear reactors to maintain the core temperature within a safe range, as efficient cooling is required to prevent the reactor core from overheating or meltdown. Liquid metals tend to have high thermal conductivity, which results in low Prandtl number values. Consequently, the cooling characteristics of liquid metals differ from those of more conventional cooling fluids. Therefore, the study of their thermal flow dynamic behaviour is necessary, especially in turbulent flows. Some conventional measurement methods, such as particle image velocimetry (PIV), cannot be used on liquid metals [5]. Use of numerical approaches, to solve the Reynolds-averaged Navier-Stokes (RANS) equations together with fairly simple eddy-viscosity based turbulence models, is still a widely employed method for predicting such complex industrial flows. However, the standard turbulent heat flux model employed in such models has typically been developed for fluids with Prandtl numbers around 1, and therefore may not be so accurate when simulating liquid metal flows with low molecular Prandtl numbers. Conducting a thorough assessment of a proposed turbulent Prandtl number model through computations of forced convection flows covering a range of low Prandtl number fluids can solve this issue in the current research. All the models are implemented in the open-source code OpenFOAM.

Section 2 mainly introduced the RANS approach and low-Reynolds-number turbulence models and models for the proposed turbulent heat fluxes employed in the present study. In Section 3, the resulting thermal models are applied to the computation of forced convection in a straight channel flow with uniform heat flux heating. The effectiveness of the proposed  $Pr_t$  model is assessed through comparisons

with DNS data. In Section 4, a backward-facing step in a turbulent forced convection regime at a Reynolds number of 4805 and over a range of Prandtl numbers is presented. The benefits of adding the standard and modified Yap correction terms to the Launder-Sharma  $k\varepsilon$  model for non-equilibrium flows are displayed. Also, various  $Pr_t$  models are tested. In Section 5, for an impinging jet at  $Re = 5700$ , both the modified Yap term and the proposed turbulent Prandtl number model at  $Pr = 0.01, 0.1$  and  $1.0$  are presented. Finally, Section 6 presents the conclusions of the current outcomes and the suggestions.

## 2 Methodology

### 2.1 RANS approach

The time-averaged Navier-Stokes equations, derived from Reynolds decomposition, form the RANS equations that describe turbulent fluid motion and include additional terms for the Reynolds stress tensor and turbulent heat flux vector, which require modelling. The Reynolds-averaged transport equations can be written as follows:

$$\frac{\partial U_i}{\partial x_i} = 0 \quad (1)$$

$$\frac{\partial U_i}{\partial t} + U_j \frac{\partial U_i}{\partial x_j} = -\frac{1}{\rho} \frac{\partial P}{\partial x_i} + \frac{\partial}{\partial x_j} \left[ \nu \left( \frac{\partial U_i}{\partial x_j} + \frac{\partial U_j}{\partial x_i} \right) - \overline{u'_i u'_j} \right] \quad (2)$$

$$\frac{\partial T}{\partial t} + U_j \frac{\partial T}{\partial x_j} = \frac{\partial}{\partial x_j} \left[ \alpha \frac{\partial T}{\partial x_j} - \overline{u'_j \theta'} \right] \quad (3)$$

The additional terms Reynolds stresses  $\overline{u'_i u'_j}$  and turbulent heat flux  $\overline{u'_j \theta'}$  arise from the Reynolds averaging process due to the non-linear nature of the convection terms.

### 2.2 Eddy viscosity turbulence modelling

Eddy viscosity turbulence models originate from the analogy between laminar and turbulent. The turbulent Reynolds stress tensor  $\overline{u'_i u'_j}$  is approximated by the Boussinesq assumption as:

$$\overline{\rho u'_i u'_j} = \frac{2}{3} \rho k \delta_{ij} - \mu_t \left( \frac{\partial U_i}{\partial x_j} + \frac{\partial U_j}{\partial x_i} \right) \quad (4)$$

where  $\delta_{ij}$  is the Kronecker delta, which is 1 when  $i = j$  and 0 otherwise,  $k$  is the turbulent kinetic energy, defined as  $k = \frac{1}{2} \overline{u'_i u'_i}$ , and  $\mu_t$  is the eddy or turbulent viscosity.

The low-Reynolds-number turbulence model, such as the Launder-Sharma  $k - \varepsilon$  model [6], is applied in this study. The turbulent viscosity in the L-S  $k - \varepsilon$  model is obtained as follows:

$$\nu_t = c_\mu f_\mu \frac{k^2}{\tilde{\varepsilon}} \quad (5)$$

where  $f_\mu$  is a damping function, and variable  $\tilde{\varepsilon}$  is the 'quasi-homogeneous' dissipation rate of  $k$

The expression of  $\nu_t$  in Equation (5) often yields excessively high turbulent length-scale values in flow regions characterised by phenomena such as separation, reattachment, or impingement, typical in adverse pressure gradient boundary layer flows. The separation may be delayed or prevented due to the large length scales, resulting in increased eddy viscosity and excessively high heat transfer estimates. This issue is typically addressed by introducing an extra near-wall source term into the Launder-Sharma version of the dissipation rate equation when the turbulent length scale is appreciably above the local equilibrium level. The adjustment follows the initial recommendation proposed by [7] based on the wall distance  $y_w$ , and is written as:

$$S_\varepsilon = \text{Yap} = 0.83 \frac{\tilde{\varepsilon}^2}{k} \max \left[ (\ell/\ell_e - 1) (\ell/\ell_e)^2, 0 \right] \quad (6)$$

where  $\ell = k^{3/2}/\tilde{\varepsilon}$  is the turbulent length scale, the equilibrium length scale  $\ell_e = 2.55y_w$ , and  $y_w$  is the wall distance. In some cases, the effect of the standard Yap term is too strong, resulting in Nusselt numbers being lower than DNS data.

By combining Equation (6) with Equation (7), the Yap term can be tailored to operate effectively at

high  $Re_t$  rather than low  $Re_t$ , enabling its functionality in proximity to the wall.

$$f_y = \max \left[ 1 - \left( \frac{Re_t}{A} \right)^n, 0 \right] \quad (7)$$

After various permutations and selections, the final choice is  $A = 200$  and  $n = 2$ .

The modified Yap term, shown below, is employed for the subsequent simulations:

$$S_\varepsilon = \text{Yap} = f_y \times 0.83 \frac{\tilde{\varepsilon}^2}{k} \max \left[ (\ell/\ell_e - 1) (\ell/\ell_e)^2, 0 \right] \quad (8)$$

The form shown seems to switch the Yap term off at high  $Re_t$ . When  $Re_t$  approaches 200, the constant  $f_y$  becomes zero, resulting in the removal of the source term  $S_\varepsilon$  from the transport equation of  $\tilde{\varepsilon}$ . In low Prandtl number flows, the region away from the wall is primarily influenced by heat transfer. Therefore, the effect of the Yap term is less significant in these cases.

Moreover, the  $k - \omega$  shear stress transport (SST) model [8] is a combination of the  $k - \varepsilon$  model employed away from the wall and the  $k - \omega$  model near the walls without the need for any additional damping functions. This model is also applied to cases involving backward-facing steps and planar impinging jets.

### 2.3 Development of turbulent Prandtl number correlation for low molecular Prandtl numbers

The turbulent heat flux term  $\overline{\theta' u'_j}$  in Equation (3) needs a closure. The most commonly used method to close the equation, especially when the dynamic field is modelled using effective-viscosity models, is as follows:

- The eddy diffusivity model, also known as the Simple Gradient Diffusion Hypothesis (SGDH), is a one-point closure model for turbulent heat flux ( $\overline{\theta' u'_i}$ ):

$$\overline{\theta' u'_i} = - \frac{\nu_t}{Pr_t} \frac{\partial T}{\partial x_i} \quad (9)$$

where  $\nu_t = \frac{C_\mu k^2}{\varepsilon}$  is the eddy viscosity and  $Pr_t$  is the turbulent Prandtl number. The turbulent Prandtl number is not a constant for low Prandtl number fluids [9]. Consequently, correlations for turbulent Prandtl numbers in terms of rational local flow quantities need to be developed for turbulent heat convection analysis involving low Prandtl number fluids. At molecular Prandtl numbers less than unity, the value of the turbulent Prandtl depends primarily on the value of the molecular Prandtl number, the value of the dimensionless wall distance,  $y^+$  and to a lesser degree on the value of the flow Reynolds number. In contrast to  $y^+$ , which is based on the absolute distance  $y$  from the wall, the local turbulence Reynolds number is expressed as  $Re_t = \frac{k^2}{\nu \varepsilon}$ . This parameter proves to be more versatile in handling complex geometries, particularly irregular shapes. In scenarios involving multiple surfaces, like wavy walls,  $y^+$  may struggle to accurately identify the closest distance to the wall. This limitation arises because  $y^+$  is linked to the variable  $y$ , and on irregular surfaces,  $y$  alone may not effectively represent the proximity to the wall. Therefore, the introduction of the turbulence Reynolds number ( $Re_t$ ) serves as a substitute, ensuring a more accurate determination of the closest distance to the wall in such situations.

In the straight channel case, consider DNS data for the turbulent Prandtl number across seven different molecular Prandtl numbers ranging from 0.007 to 0.71 at a Reynolds number based on wall friction velocity ( $Re_\tau$ ) of 1000 [1]. Use curve-fitted  $Pr_t$  values as a function of  $y^+$  to derive various correlations. Specifically,  $y^+$  was replaced by  $\min[BRe_t^2, 4000]$  as explained earlier. These  $Pr_t$  correlations represent different relationships for various ranges of  $y^+$ , with specific values for  $Pr_{t1}$  to  $Pr_{t5}$ ,  $m_1$  to  $m_3$  and  $b_1$  to  $b_3$  displayed in Table 1.

For  $\min[BRe_t^2, 4000] < 5.5$

$$Pr_t = m_0 \min [BRe_t^2, 4000] + b_0$$

For  $5.5 < \min [BRe_t^2, 4000] < 45$

$$Pr_t = (m_1 \min [BRe_t^2, 4000] + b_1)$$

For  $45 < \min [BRe_t^2, 4000] < 135$

$$Pr_t = (m_2 \min [BRe_t^2, 4000] + b_2)$$

For  $135 < \min [BRe_t^2, 4000] < 1000$

$$Pr_t = (m_3 \min [BRe_t^2, 4000] + b_3)$$

For  $1000 < \min [BRe_t^2, 4000]$

$$Pr_t = Pr_{t5} + (Pr_{t4} - Pr_{t5}) \exp[-(\min [BRe_t^2, 4000] - y_4^+)]$$

Since the above formulas are primarily derived from DNS data for  $Pr_t$  at  $Re_\tau = 1000$ , further modifications are needed for  $Pr_t$  values at lower Reynolds numbers, like  $Re_\tau = 180$ .

$$Pr_t^c = 0.85 \times [1 - \min((\frac{Re_t}{185})^{10}, 1.0)] + Pr_t \times \min((\frac{Re_t}{185})^{10}, 1.0) \quad (10)$$

After adding Equation (10), this calculation for  $Pr_t$  underestimates the Nusselt numbers, particularly for moderate Prandtl numbers at higher Reynolds numbers. Furthermore, it considers the application of more complex geometries. Therefore, further modifications are needed, as shown below:

For  $Re_t < 75$

$$Pr_t^c = Pr_t \quad (11)$$

For  $Re_t > 75$

$$Pr_t^c = 0.8 + \min[\max((Pr_t/1.2\varepsilon)^2, 0.4), 1.0] \times (Pr_t - 0.8) \quad (12)$$

Table 1: The correlations of the proposed  $Pr_t$  model.

<b>The values of <math>Pr_{t0}</math>, <math>Pr_{t1}</math>, <math>Pr_{t2}</math>, <math>Pr_{t3}</math>, <math>Pr_{t4}</math> and <math>Pr_{t5}</math> from:</b>
$Pr_{t0} = \max\left(0.9, 0.98 - \frac{(Pr-0.05)}{0.65} \cdot 0.08, 1.8 - \frac{(Pr-0.02)}{0.03} \cdot 0.82, 3.2 - \frac{(Pr-0.01)}{0.01} \cdot 1.4, 4.45 - \frac{(Pr-0.007)}{0.003} \cdot 1.25\right)$
$Pr_{t1} = \max\left(1.02, 1.5 - \frac{(Pr-0.05)}{0.65} \cdot 0.48, 2.4 - \frac{(Pr-0.02)}{0.03} \cdot 0.9, 4.4 - \frac{(Pr-0.01)}{0.01} \cdot 2, 6.2 - \frac{(Pr-0.007)}{0.003} \cdot 1.8\right)$
$Pr_{t2} = \max\left(1.04, 1.5 - \frac{(Pr-0.05)}{0.65} \cdot 0.46, 2.25 - \frac{(Pr-0.02)}{0.03} \cdot 0.75, 3.8 - \frac{(Pr-0.01)}{0.01} \cdot 1.55, 5 - \frac{(Pr-0.007)}{0.003} \cdot 1.2\right)$
$Pr_{t3} = \max\left(0.95, 1.4 - \frac{(Pr-0.05)}{0.65} \cdot 0.45, 1.7 - \frac{(Pr-0.02)}{0.03} \cdot 0.3, 2.4 - \frac{(Pr-0.01)}{0.01} \cdot 0.7, 3 - \frac{(Pr-0.007)}{0.003} \cdot 0.6\right)$
$Pr_{t4} = \max\left(0.9, 1.5 - \frac{(Pr-0.02)}{0.03} \cdot 0.25, 1.2 - \frac{(Pr-0.02)}{0.03} \cdot 0.05, 1.25 - \frac{(Pr-0.01)}{0.01} \cdot 0.05, 1.7 - \frac{(Pr-0.007)}{0.003} \cdot 0.45\right)$
$Pr_{t5} = \max\left(0.9, 1.1 - \frac{(Pr-0.05)}{0.65} \cdot 0.2, 1.15 - \frac{(Pr-0.02)}{0.03} \cdot 0.05, 1.2 - \frac{(Pr-0.01)}{0.01} \cdot 0.45, 1.4 - \frac{(Pr-0.007)}{0.003} \cdot 0.2\right)$
<b>The values of <math>m_0</math>, <math>m_1</math>, <math>m_2</math>, <math>m_3</math>, <math>b_0</math>, <math>b_1</math>, <math>b_2</math> and <math>b_3</math> from:</b>
$m_0 = \frac{(Pr_{t1}-Pr_{t0})}{y_1^+}, b_0 = Pr_{t0}$
$m_1 = \frac{(Pr_{t2}-Pr_{t1})}{y_2^+-y_1^+}, b_1 = \frac{y_2^+ Pr_{t1}-y_1^+ Pr_{t2}}{y_2^+-y_1^+}$
$m_2 = \frac{(Pr_{t3}-Pr_{t2})}{y_3^+-y_2^+}, b_2 = \frac{y_3^+ Pr_{t2}-y_2^+ Pr_{t3}}{y_3^+-y_2^+}$
$m_3 = \frac{(Pr_{t4}-Pr_{t3})}{y_4^+-y_3^+}, b_3 = \frac{y_4^+ Pr_{t3}-y_3^+ Pr_{t4}}{y_4^+-y_3^+}$

### 3 Model Development in Plane Channel Flow

The fully-developed turbulent flow and heat transfer in a plane channel has been studied initially, making use of an available DNS database of the flow and heat transfer over a range of moderate and low molecular Prandtl numbers [1]. The geometry of a straight channel is illustrated in Figure 1. The flow is considered incompressible and in a steady state. In this case, the domain and the flow are two-dimensional. The computational domain dimensions are  $L = 65\text{ m}$  and  $H = 1\text{ m}$  in the stream-wise and wall-normal directions respectively. The channel is long enough in the stream-wise direction to ensure that the flow field becomes fully developed in the downstream region. The no-slip conditions are on both walls. A zero-gradient inlet condition was applied to the pressure while it was maintained at a reference value of zero at the outlet. The flow is heated by a uniform heat flux from the upper and lower walls. The steady RANS approach is adopted here, fully developed state, and comparisons are performed against the DNS data from [9] and [1].

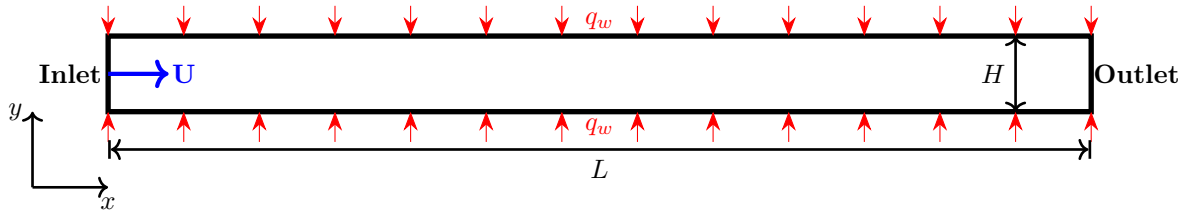


Figure 1: Geometry for a two-dimensional fully developed straight channel flow case.

The channel flows considered here ranged in Reynolds number based on the wall shear stress from  $Re_\tau = 180$  up to 2000 and in Prandtl number from  $Pr = 0.007$  to 0.7. As illustrative results, Figure 2 shows comparisons of mean temperature profiles for six Prandtl numbers at the highest Reynolds number  $Re_\tau = 2000$ . These comparisons confirm that the proposed model consistently improves the accuracy of the thermal predictions (assessed through comparisons with DNS data) relative to the predictions resulting from the use of a constant turbulent Prandtl number the so-called Kays correlation [2].

Figure 3 shows comparisons of the Nusselt number for a range of Prandtl numbers at  $Re_\tau = 180$  to 2000. Also included for comparison are results using the standard constant-value turbulent Prandtl number of 0.85 and the Kays correlation [2]. The resulting comparisons are consistent with the mean temperature profiles. They demonstrate that the introduction of the proposed model for the turbulent Prandtl number brings the predicted levels of the Nusselt number to close agreement with the DNS over the entire range of Prandtl and Reynolds numbers tested for low-Reynolds-number turbulence models. By contrast, the more conventional use of a constant value for the turbulent Prandtl number at the higher Reynolds numbers results in an over-estimation of the DNS's Nusselt number levels, which at the lower molecular Prandtl number tested (0.007) is as high as 30%. These comparisons provide further support for the use of the proposed model for the turbulent Prandtl number for heat convection analysis in fluids of low molecular Prandtl number.

### 4 Model Development in backward-facing step

After implementing the proposed turbulent Prandtl number model successfully in a straight channel, more complex configurations have been considered, including a backward-facing step (BFS). The 2D computational case involves simulating flow over a backward-facing step, where the jet width is represented by  $2h$ , as depicted in Figure 4. The origin of the coordinate system is situated at point  $o$ . The downstream channel has a  $H$  height equal to  $3h$ , resulting in an expansion ratio (wind tunnel height ratio before and after the step) of  $ER = H/(H - h) = 1.5$ . The dimensions of the computational domain for the backward-facing step are  $34h$  in the stream-wise direction (denoted by spatial coordinate  $x$ ) and  $3h$  in the wall-normal direction (denoted by spatial coordinate  $y$ ). At the inlet, a fully developed channel flow with an inlet temperature set to  $T_{in} = 423.15\text{ K}$  is imposed, which is located  $4h$  upstream of the step. Beyond the step, the bottom wall is heated by a uniform heat flux density  $\dot{q}$  for a length of  $20h$ . No-slip conditions are applied on both the up and bottom walls. Precursor simulations were conducted to establish a fully developed channel flow that could be applied as inlet conditions. At the outlet boundary, zero gradient conditions were applied for velocity and turbulent quantities. A zero-gradient inlet condition was applied to the pressure while it was maintained at a reference value of

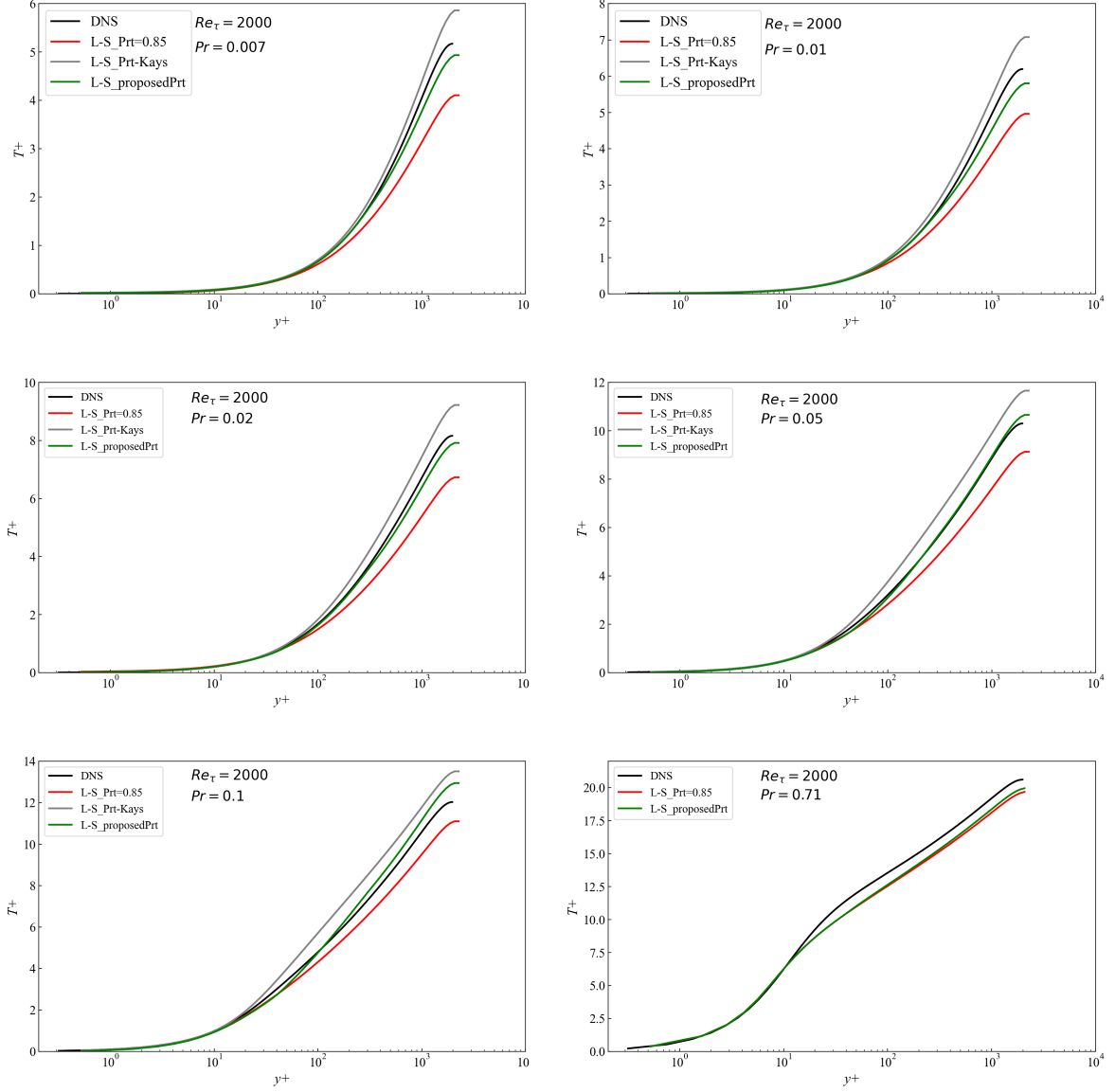


Figure 2: Non-dimensional temperature profiles for  $Re_\tau = 2000$ . Comparisons between L-S with different  $Pr_t$  correlations and DNS (black lines) of [9, 1].

zero at the outlet. The bulk Reynolds numbers,  $Re = \frac{U_{bulk} h}{\nu} = 4805$ , is established based on the bulk velocity ( $U_{bulk} = 1.0 \text{ m/s}$ ) and half the jet width ( $h$ ). The computations are performed for four Prandtl numbers:  $Pr = 0.01, 0.025, 0.1, \text{ and } 1.0$ .

Contours of mean stream-wise velocity are shown in Figure 5. At the reattachment location,  $U/U_{bulk} = 0$ , also reflected in the streamlines. When the flow reattaches to the downstream wall, positive velocities are observed again in the downstream region. Comparing the reattachment point of DNS (around  $x = 6.5 h$ ) with the L-S  $k - \varepsilon$  (around  $x = 7.8 h$ ) and SST  $k - \omega$  model (around  $x = 7.0 h$ ) results, the reattachment point is predicted further downstream by the L-S  $k - \varepsilon$  model. All simulations exhibit negative velocities in the recirculation region due to the flow reversing direction. The secondary circulation vortex in the step corner forms because the momentum of the near-wall fluid in the main recirculation, directed towards the corner, is insufficient to overcome the adverse pressure gradient due to the vertical step wall. Furthermore, the secondary recirculation region by the L-S  $k - \varepsilon$  model is noticeably smaller than that from the SST  $k - \omega$  model and DNS one. This suggests the low- $Re$   $k - \varepsilon$  model may not accurately capture the intricate details of the turbulence in the separation region here. Conversely, the SST  $k - \omega$  model exhibits superior performance in this scenario.

As can be seen from Figure 6 to 8, mean temperature contours with DNS and RANS models are

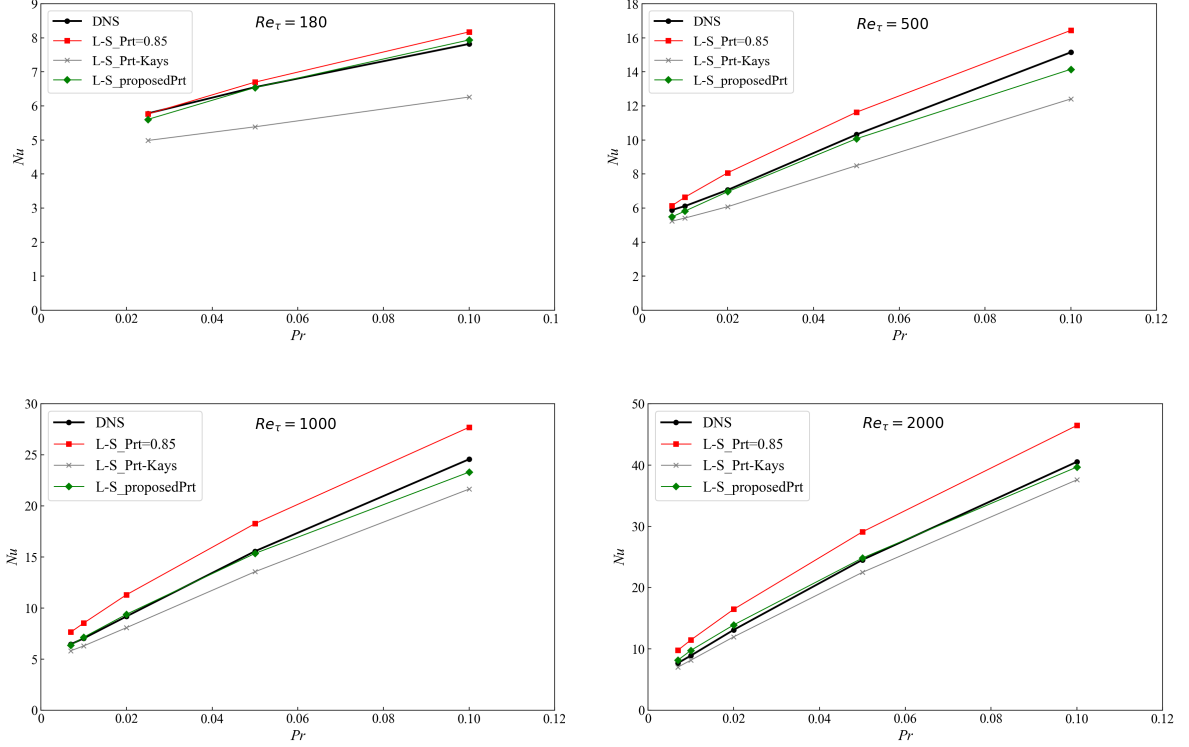


Figure 3: Mean Nusselt numbers on the bottom wall. Comparisons between L-S with different  $Pr_t$  correlations and DNS (black lines) [9, 1].

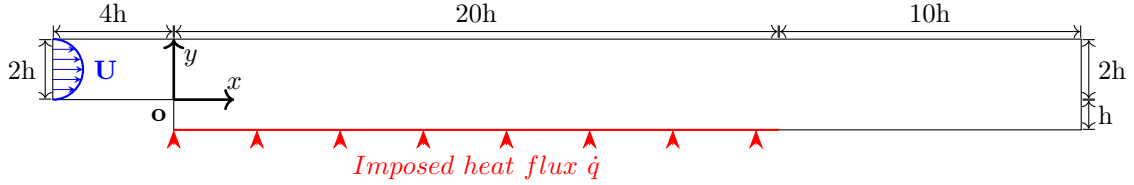


Figure 4: Geometry for a two-dimensional backward-facing step flow case with  $Re$  of 4805.

displayed for four Prandtl numbers. The recirculation zone has the highest temperature values. This is because, in comparison to other flow field regions, flow close to the step is characterized by slower velocities and longer residence duration, which allow heat to build up and result in higher temperatures. It is evident that as the Prandtl number reduces, the thermal boundary layer thickens. This observation is consistent with the fundamental principles of convective heat transfer, where a lower Prandtl number indicates a stronger molecular thermal diffusion relative to momentum diffusion. The thermal boundary layer expands in the recirculating regions. This expansion leads to lower temperature gradients due to the spread of temperature differences over a larger distance at low Prandtl numbers (when  $Pr = 0.01$ ). All temperature contours are generated using the same proposed  $Pr_t$  model. In Figure 6, it can be observed that the highest temperature values from  $x/h = 0$  to 3 when employing the L-S  $k - \varepsilon$  model are greater than those obtained with DNS and the SST  $k - \omega$  model. However, as contours may not accurately depict near-wall temperature differences, the subsequent Nusselt number profiles provide a clearer comprehension.

Figure 9 depicts the profiles of the Nusselt number ( $Nu = \frac{\dot{q}h}{(T_w - T_{in})\lambda}$ , where  $\lambda$  is the thermal conductivity of the flow, and the characteristic length is half the inlet channel height) for four different Prandtl numbers ( $Pr = 0.01, 0.025, 0.1, \text{ and } 1.0$ ).

Looking at comparisons of the different turbulence models with the same  $Pr_t$  model, it becomes evident that the SST  $k - \omega$  model exhibits better agreement with DNS data in the recirculation region. Specifically, from  $x/h = 0$  to 3, the Nusselt number with the SST  $k - \omega$  model closely follows the shape of the DNS result. However, beyond  $x/h = 3$ , the SST  $k - \omega$  model notably underestimates the

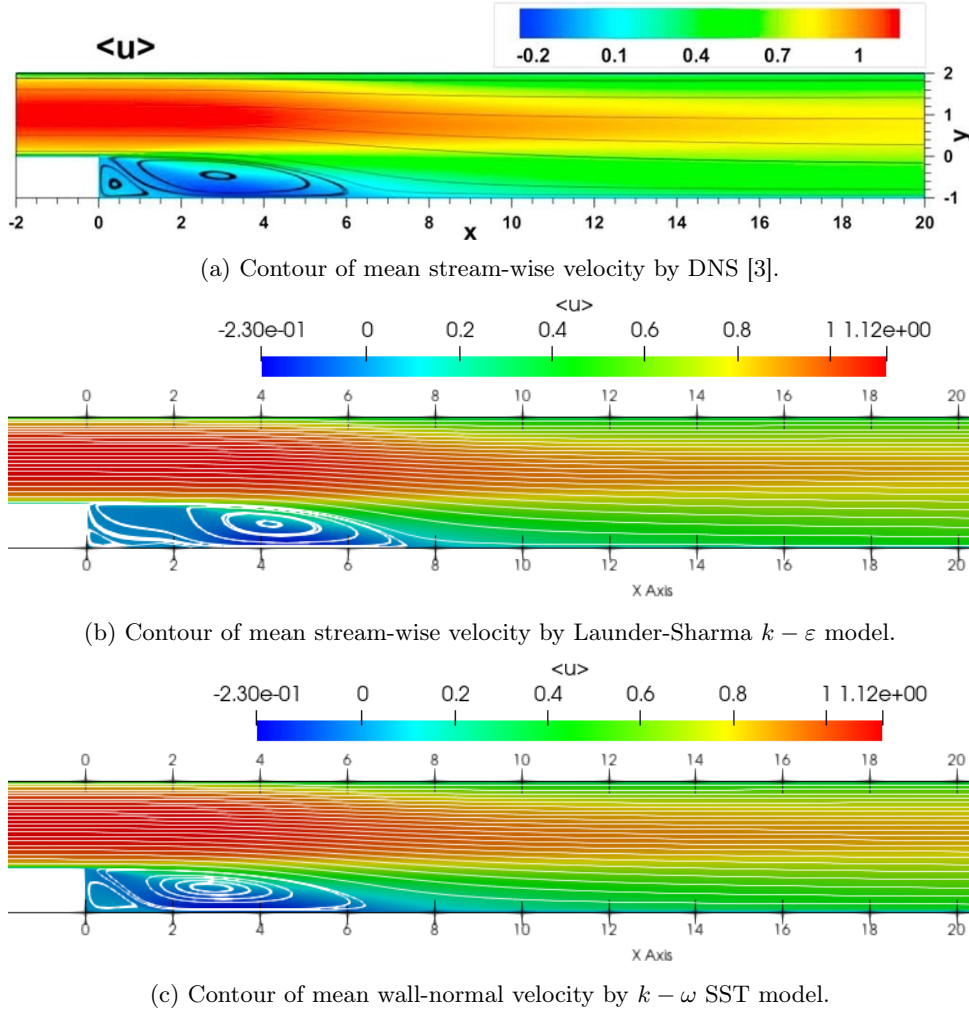


Figure 5: Contours of mean stream-wise velocity.

DNS data, falling below the results obtained with the L-S  $k - \epsilon$  model with various length corrections. This discrepancy is attributed to the SST  $k - \omega$  model's inability to accurately capture near-wall mean temperature differences compared to the L-S  $k - \epsilon$  model with various length corrections. As the Prandtl number increases, the ratio of momentum diffusion to thermal transport in the flow becomes more significant, thereby amplifying the effect of the Yap term. However, for  $Pr = 0.01$  and  $0.1$ , the standard Yap term in the L-S  $k - \epsilon$  model excessively reduces turbulence. The modified Yap term effectively mitigates this effect and demonstrates better agreement with the DNS data. In summary, although the L-S  $k - \epsilon$  model with modified Yap term may not accurately capture the upstream vortex, the overall results exhibit the best agreement with DNS data.

The Nusselt number profiles were obtained using three different  $Pr_t$  models with the same turbulence model (L-S  $k - \epsilon$  model with the modified Yap term), as shown in right-hand-side of Figure 9. The dynamic field does not agree well with DNS data due to their reliance on an imperfect turbulence model. Therefore, the discrepancies in the Nusselt number profiles based on the imperfect turbulence model are relatively reasonable. In general, the proposed  $Pr_t$  model demonstrates good agreement with DNS data. Although, for  $0.01$ , the proposed  $Pr_t$  model underestimates the DNS results, the underlying turbulence model was also seen earlier to underestimate the levels of turbulence in the near-wall recirculation region. On the other hand, when the turbulence model achieves good agreement with DNS data, such as for  $Pr = 0.025$  and  $0.1$ , the proposed  $Pr_t$  model exhibits the best performance among the  $Pr_t$  models, where the modified Yap term also performs best in the early estimations for different turbulence models. Considering all the profiles for Nusselt numbers, the optimal combination for this backward-facing step case appears to be the L-S  $k - \epsilon$  model with a modified Yap term and proposed  $Pr_t$  model.

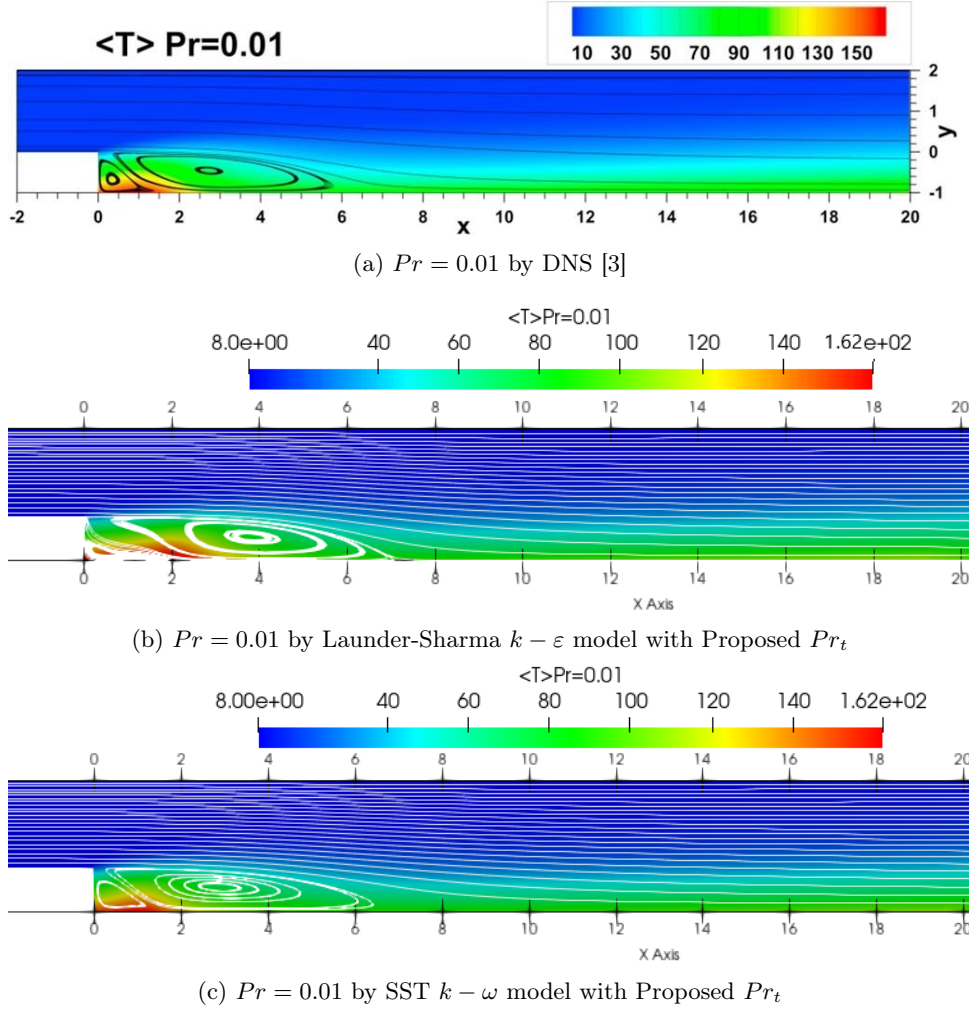


Figure 6: Contour of mean temperature for  $Pr = 0.01$ .

## 5 Model Development in planar impinging jet

The 2D computational case involves simulating flow within a planar impinging jet, as shown in Figure 10. The configuration of the planar impinging jet involves two parallel flat plates. The upper plate is divided by a slit, allowing a fully-developed flow to be injected to generate the jet. This jet impinges on the lower plate, which subsequently exits the domain through two outlet segments. In this case, the computational planar impinging jet domain dimensions are  $L = 80 B$  and  $H = 2 B$  in the wall-parallel and wall-normal directions, respectively. The upper surface also includes the slit ( $y = H$  and  $-B/2 < x < B/2$ )

The upper and lower walls are iso-thermal so that  $T = T_w$  is applied to the walls. In the slit ( $y = H$  and  $|x| < B/2$ ), the uniform temperature  $T = T_j$  is imposed on the incoming flow. The temperature difference between the jet and the walls is expressed as  $\Delta T = T_j - T_w$ . Due to the geometric axis symmetry of the fluid domain, the symmetry boundary condition can be applied on the central line ( $x = 0$ ), and only half the domain shown in Figure 10 is employed. No-slip conditions are applied on both the upper and bottom walls. Precursor simulations are conducted to establish a fully developed channel flow before it enters the step zone. Zero gradient conditions were applied at the outlet boundary for velocity and turbulent quantities. Meanwhile, a zero-gradient inlet condition was applied to the pressure while it was maintained at a reference value of zero at the outlet.

The bulk Reynolds numbers,  $Re = \frac{U_{bulk} B}{\nu} = 5700$ , where  $U_{bulk}$  is bulk velocity, is established based on the bulk velocity ( $U_{bulk} = 1.0$  m/s) and the jet width ( $B$ ). The computations are performed for three Prandtl numbers:  $Pr = 0.01$ ,  $0.1$ , and  $1.0$ .

Figure 11 display the instantaneous temperature ( $(T - T_w) / (T_j - T_w)$ ) contours between DNS data and the L-S  $k - \varepsilon$  with proposed  $Pr_t$  model for three distinct Prandtl numbers ( $Pr = 1.0$ ,  $0.1$ , and  $0.01$ ). For  $Pr = 1$  as shown in Figure 11, the thickness of the thermal boundary layer is very close to that of the

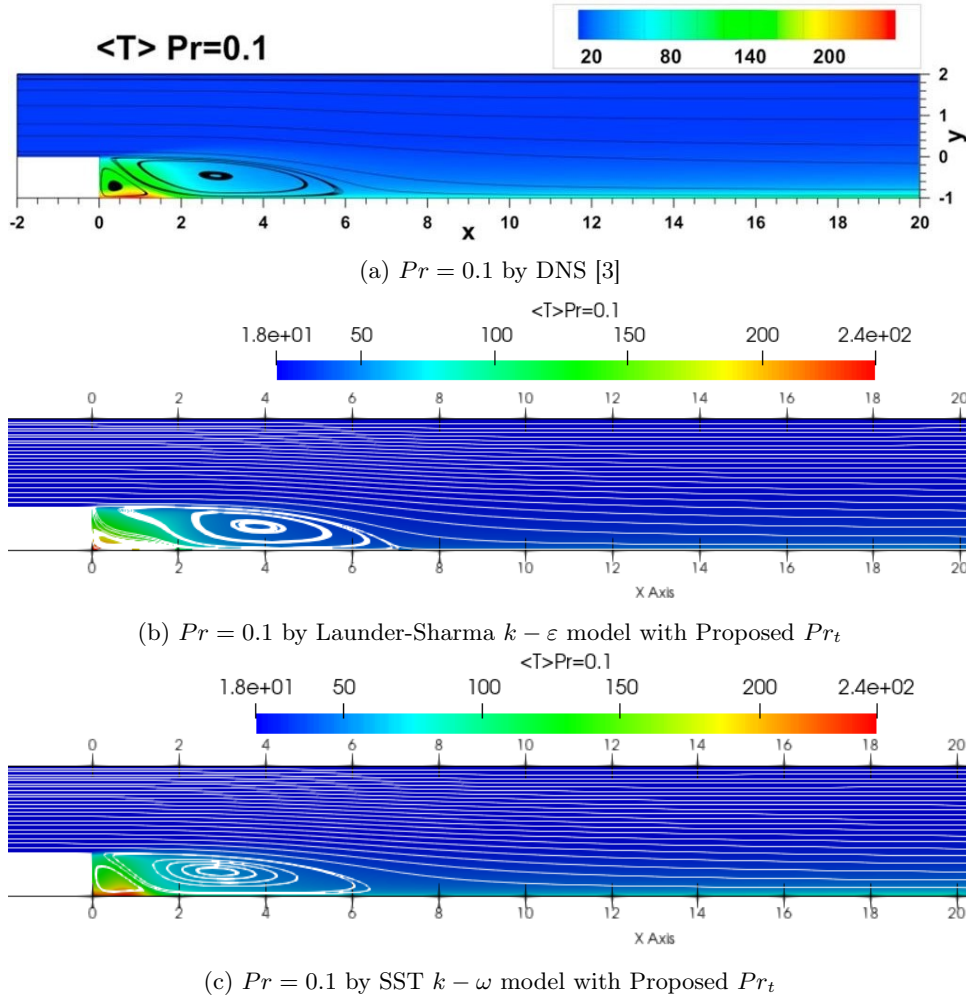


Figure 7: Contour of mean temperature for  $Pr = 0.1$ .

velocity boundary layer. As the Prandtl number decreases, the thickness of the thermal boundary layer increases. Furthermore, the heat is more efficiently conducted away from hotter areas and distributed throughout the domain, as observed in the contour plots, at lower  $Pr$ . The trends between the DNS result and RANS models align well for all  $Pr$ .

The Nusselt number ( $Nu = \frac{q_w B}{\lambda \Delta T}$ , where  $q_w$  is the wall heat flux) that is determined along the lower plate is shown in Figure 12. The DNS results in all present a peak value at the stagnation point ( $x/B = 0$ ), and a small secondary peak can be seen at approximately  $x/B = 4$  for  $Pr = 1$ , corresponding roughly to where the weak inflection point in the  $C_f$  profile was seen earlier. Then, when the flow approaches the outlet section,  $Nu$  starts to decline. The left-hand side of Figure 12 shows results from the L-S  $k - \varepsilon$  model with three different length scale corrections at  $Pr = 1$ . Without adding the Yap term, the  $k - \varepsilon$  model overestimates the turbulent energy in the stagnation region due to the non-equilibrium flow. The Yap term decreases the turbulent kinetic energy level by increasing  $\varepsilon$ , resulting in improvements in the accuracy of the prediction of  $Nu$ . The peak  $Nu$  value at the stagnation point returned by the model without the Yap term is approximately twice that returned by the models with a length scale correction. Both forms of the length scale correction lead to a much lower stagnation point  $Nu$ , with a small peak located just off the symmetry plane of the jet, at around  $x/B = 0.5$ . Moving away from the stagnation region, all the models with different length scale corrections return results that are close to each other. At  $Pr = 0.01$  and  $0.1$ , it is evident that the effect of the Yap term reduces as  $Pr$  decreases and no secondary peak of  $Nu$  is observed in the DNS data because of the heightened contribution of the molecular heat flux to the overall heat transfer.

The right-hand side of Figure 12 compares various  $Pr_t$  models using the L-S  $k - \varepsilon$  model with the modified Yap term. At  $Pr = 1$ , all the models show a higher peak to the DNS data at the stagnation point. Additionally, all the models exhibit a secondary peak in  $Nu$  at around  $x/B \approx 8$ , also seen in

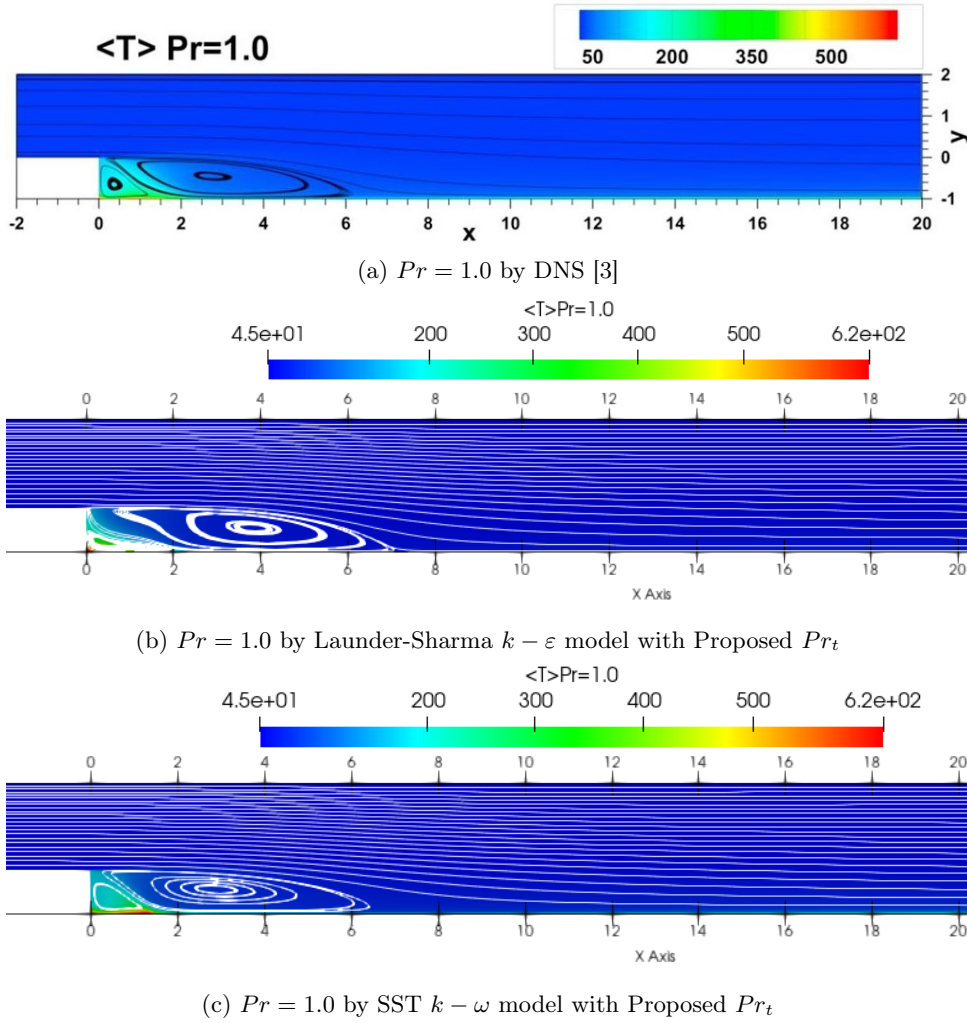


Figure 8: Contours of mean temperature for  $Pr = 1.0$ .

the wall friction coefficient profile. The Kays correlation gives a slightly lower secondary  $Nu$  peak value than the other models. In the downstream region, all the models provide a fair prediction compared to the DNS data. At  $Pr = 0.1$ , the Kays correlation shows a better agreement with DNS data at the stagnation point, although subsequently, the proposed  $Pr_t$  model results are closer to the DNS data up to around  $x/B \approx 7$ . Moving further downstream, the Kays correlation has a better prediction than the other two models from  $x/B \approx 7.5$ . As the flow moves toward the outlet section, all models return very similar values and tend to underestimate the  $Nu$  value. At  $Pr = 0.01$ , the proposed  $Pr_t$  model and Kays correlation display better agreement with DNS data than the constant  $Pr_t$  model at the stagnation point. After around  $x/B = 1$  all the  $Pr_t$  models return results very close to each other and in almost perfect agreement with the DNS data.

## 6 Conclusion and Future Work

The study investigated the influence of turbulent Prandtl number models on thermal predictions for low-Prandtl number fluids in a straight channel with uniform wall heat flux, comparing simulation results with DNS data. The proposed turbulent Prandtl number model demonstrated improved accuracy in thermal predictions compared to using a constant value or the Kays correlation across various Reynolds numbers and low Prandtl numbers considered. The study focused on forced convective heat transfer of low Prandtl number flows over a backward-facing step, revealing that the SST  $k-\omega$  model better captured flow characteristics. In contrast, the L-S  $k-\epsilon$  model with a modified Yap term and the proposed  $Pr_t$  model provided the best thermal predictions, aligning closely with DNS data across various Prandtl numbers. The study on 2-D planar impinging jet flow and heat transfer at different Prandtl numbers

( $Pr = 1.0, 0.1, 0.01$ ) demonstrated that the proposed  $Pr_t$  model with the modified Yap term generally provided the best agreement with DNS data, particularly at  $Pr = 0.01$  and  $0.1$ .

Future research should extend simulations to more complex geometries and higher Reynolds numbers, as well as develop experimental studies for detailed data, to enhance the practical application of the proposed  $Pr_t$  model in industrial liquid metal cooling systems.

## References

- [1] Francisco Alcántara-Ávila, S Hoyas, and María Jezabel Pérez-Quiles. Dns of thermal channel flow up to  $re\tau = 2000$  for medium to low prandtl numbers. *International journal of heat and mass transfer*, 127:349–361, 2018.
- [2] Wiliam M Kays. Turbulent prandtl number. where are we? *ASME Journal of Heat Transfer*, 116(2):284–295, 1994.
- [3] Pinghui Zhao, Zhihao Ge, Jiayin Zhu, Jiaming Liu, and Minyou Ye. Quasi-direct numerical simulation of forced convection over a backward-facing step: effect of prandtl number. *Nuclear Engineering and Design*, 335:374–388, 2018.
- [4] Matthieu Duponcheel and Yann Bartosiewicz. Direct numerical simulation of turbulent heat transfer at low prandtl numbers in planar impinging jets. *International Journal of Heat and Mass Transfer*, 173:121179, 2021.
- [5] Thomas Schulenberg and Robert Stieglitz. Flow measurement techniques in heavy liquid metals. *Nuclear Engineering and Design*, 240(9):2077–2087, 2010.
- [6] Brian Edward Launder and Bahrat I Sharma. Application of the energy-dissipation model of turbulence to the calculation of flow near a spinning disc. *Letters in heat and mass transfer*, 1(2):131–137, 1974.
- [7] Christopher R Yap. *Turbulent heat and momentum transfer in recirculating and impinging flow*. The University of Manchester (United Kingdom), 1987.
- [8] Menter and Christopher Rumsey. Assessment of two-equation turbulence models for transonic flows. In *Fluid Dynamics Conference*, page 2343, 1994.
- [9] Hiroshi Kawamura, Hiroyuki Abe, and Kenji Shingai. Dns of turbulence and heat transport in a channel flow with different reynolds and prandtl numbers and boundary conditions. *Turbulence, Heat and Mass Transfer*, 3:15–32, 2000.

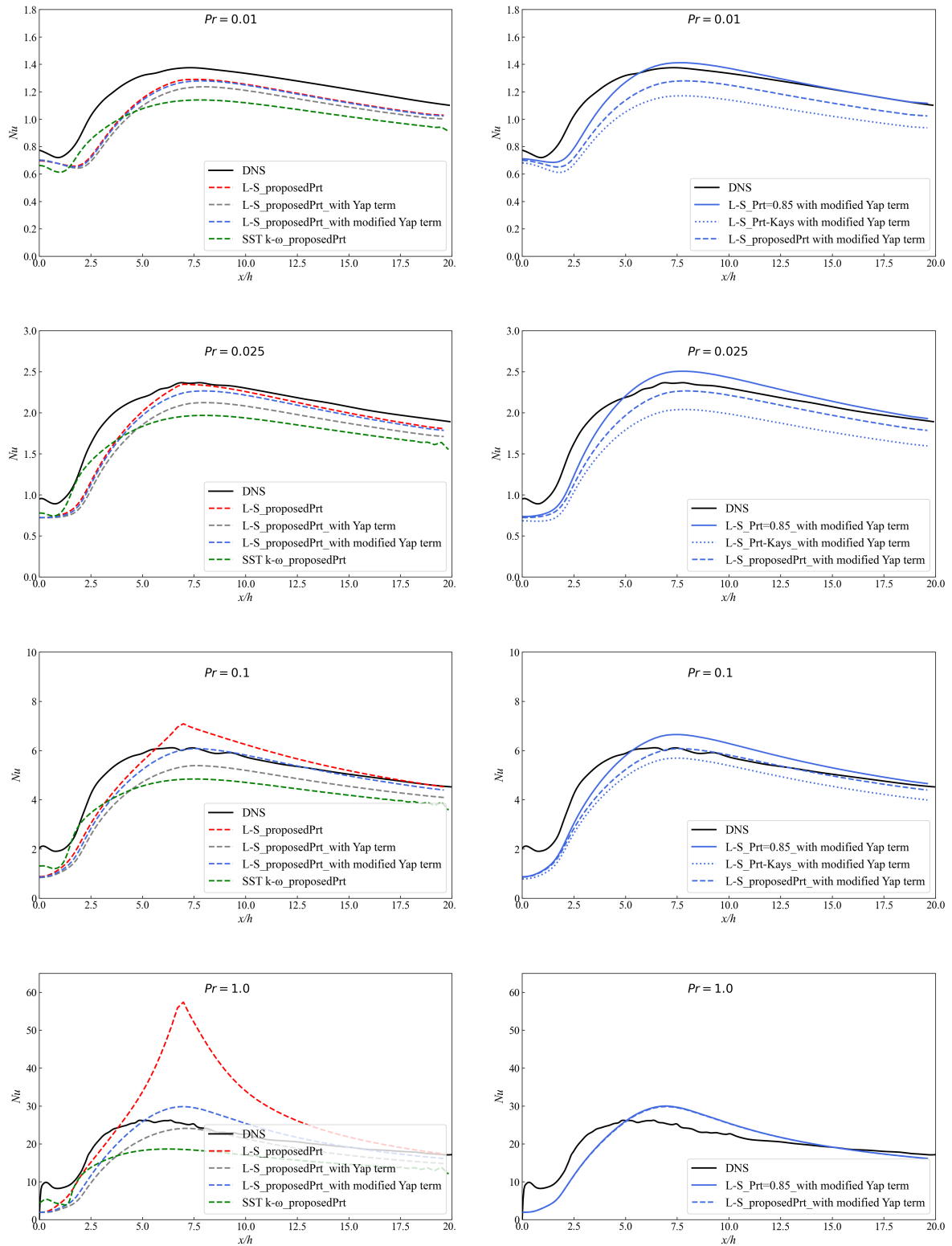


Figure 9: Non-dimensional temperature profiles of BFS for  $Re = 4805$ . Comparisons for different turbulence models with the constant  $Pr_t$  and various  $Pr_t$  correlations with a fixed turbulence model compared against DNS (black lines) [3].

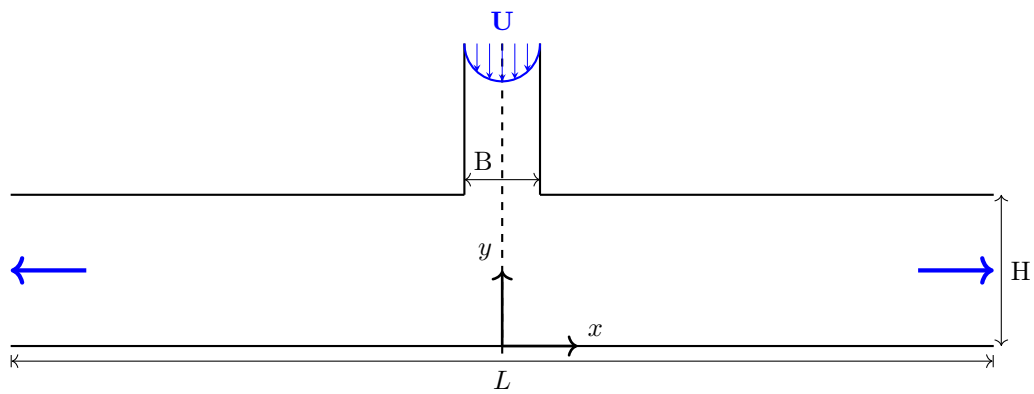
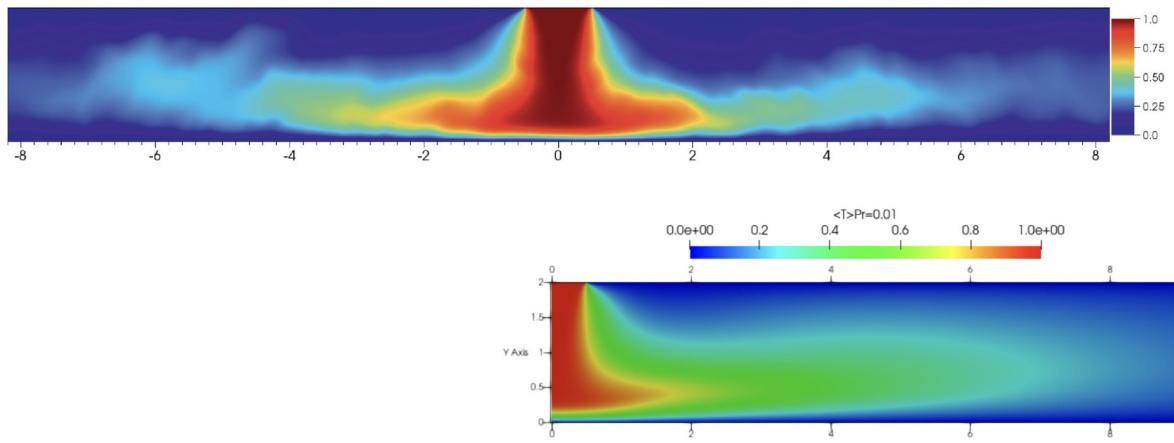


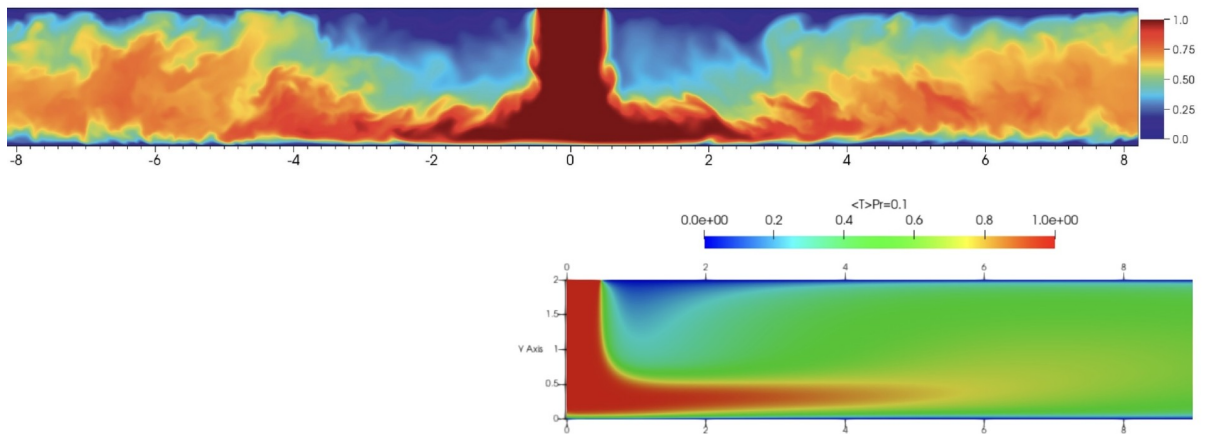
Figure 10: Geometry for a two-dimensional planar impinging jet with  $Re$  of 5700.

$$(T - T_w)/\Delta T \quad (Pr = 0.01)$$



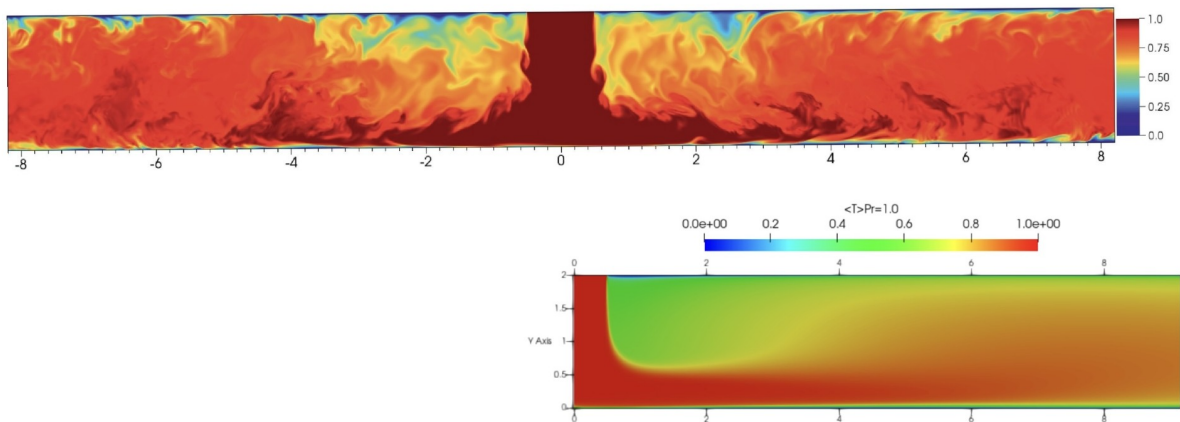
(a)  $Pr = 1.0$

$$(T - T_w)/\Delta T \quad (Pr = 0.1)$$



(b)  $Pr = 0.1$

$$(T - T_w)/\Delta T \quad (Pr = 1)$$



(c)  $Pr = 0.01$

Figure 11: Contours of mean temperature ( $\Delta T = T_j - T_w$ ) in planar impinging jets by DNS [4] (top), by Launder-Sharma  $k - \varepsilon$  model (bottom).

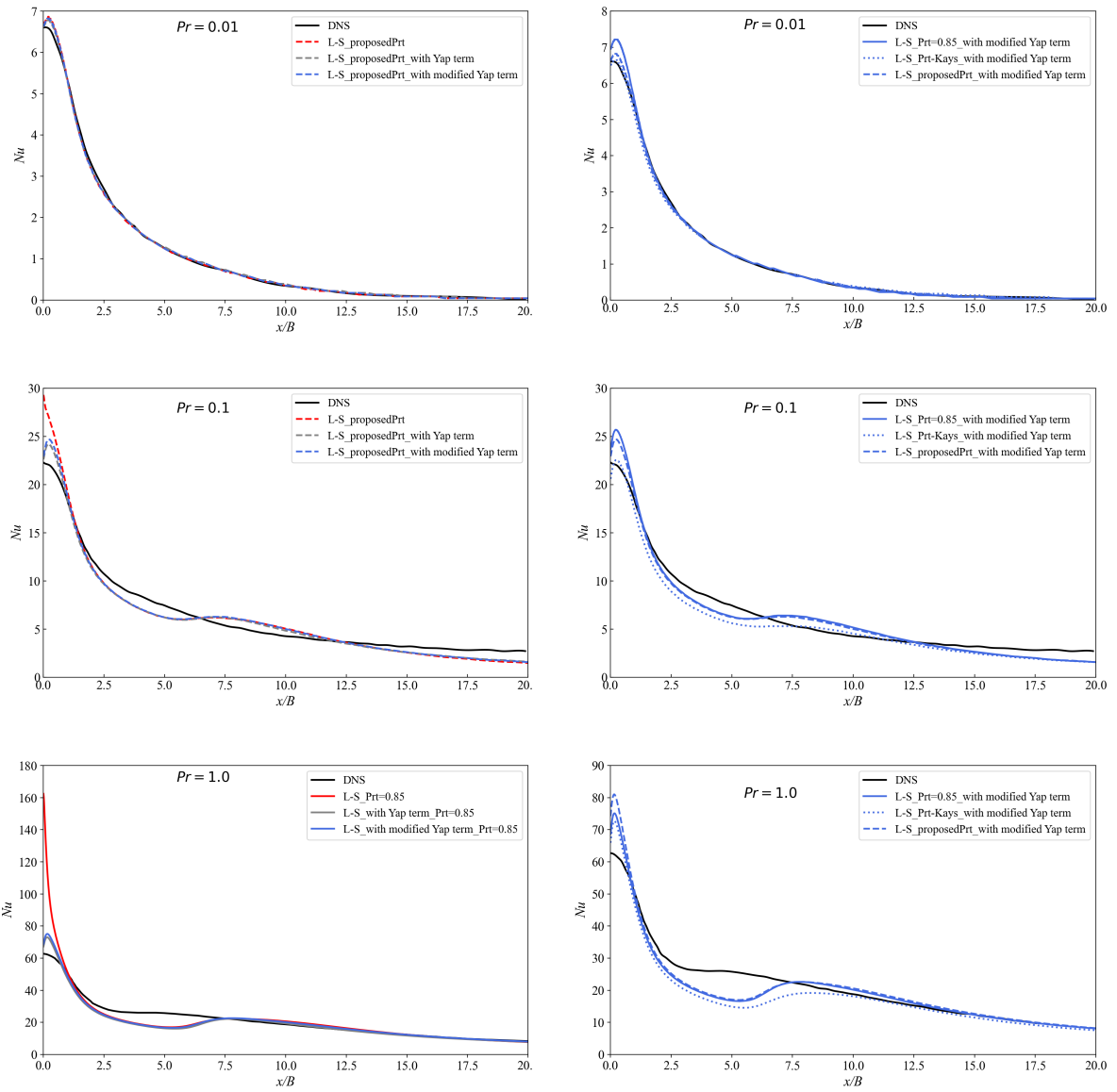


Figure 12: Local Nusselt number comparisons for a planar impinging jet at  $Re = 5700$  and  $Pr = 0.01, 0.1$  and  $1.0$ . Comparisons for different turbulence models with the constant  $Pr_t$  and various  $Pr_t$  correlations with a fixed turbulence model compared against DNS (black lines) [4].